Published in final edited form as:
*IEEE Trans Biomed Eng*. 2013 October ; 60(10): 2904–2913. doi:10.1109/TBME.2013.2265877.

# A Flexible Base Electrode Array for Intraspinal Microstimulation

**I. Khaled**,
Department of Mechanical Engineering, University of Alberta, Edmonton, Canada, T6G 2V4

**S. Elmallah**,
Department of Chemical and Materials Engineering, University of Alberta, Edmonton, Canada, T6G 2V4

**C. Cheng**,
Department of Chemical and Materials Engineering, University of Alberta, Edmonton, Canada, T6G 2V4

**W.A. Moussa**,
Department of Mechanical Engineering, University of Alberta, Edmonton, Canada, T6G 2V4

**V.K. Mushahwar*** **[Member IEEE]**, and
Division of Physical Medicine & Rehabilitation and Centre for Neuroscience, Faculty of Medicine and Dentistry, University of Alberta, Edmonton, Alberta, Canada, T6G 2E1

**A.L. Elias***
Department of Chemical and Materials Engineering, University of Alberta, Edmonton, Canada, T6G 2V4, phone:780-248-1589; fax: 780-492-2881

V.K. Mushahwar: vivian.mushahwar@ualberta.ca; A.L. Elias: aelias@ualberta.ca

## Abstract

In this paper, we report the development of a flexible base array of penetrating electrodes which can be used to interface with the spinal cord. A customizable and feasible fabrication protocol is described. The flexible base arrays were fabricated and implanted into surrogate cords which were elongated by 12%. The resulting strains were optically measured across the cord and compared to those associated with two types of electrodes arrays (one without a base and one with a rigid base connecting the electrodes). The deformation behavior of cords implanted with the flexible base arrays resembled the behavior of cords implanted with individual microwires that were not connected through a base. The results of the strain test were used to validate a 2D finite element model. The validated model was used to assess the stresses induced by the electrodes of the 3 types of arrays on the cord, and to examine how various design parameters (thickness, base modulus, etc.) impact the mechanical behavior of the electrode array. Rigid base arrays induced higher stresses on the cord than the flexible base arrays which in turn imposed higher stresses than the individual microwire implants. The developed flexible base array showed improvement over the rigid base array; however, its stiffness needs to be further reduced to emulate the mechanical behavior of individual microwire arrays without a base.



*Denotes equal contributions to senior authorship

All authors are members of the Alberta Innovates-Health Solutions Interdisciplinary Team in Smart Neural Prostheses

**Index Terms**

electrode array; spinal cord; spinal cord injury; electrical stimulation; finite element model; mechanical compliance; mechanical properties

## I. Introduction

Spinal cord injury (SCI) leads to an interruption in the neural signals between the brain and the intact motor neurons below the lesion site, and often causes the loss of function in the lower extremities [1], [2]. Intraspinal microstimulation (ISMS) is a neuroprosthetic technique that involves the implantation of micro-sized-electrodes within the spinal cord below the site of injury [3]. Electrical stimulation through these microelectrodes activates the remaining motoneuronal pools and elements of the neural networks involved in locomotion, thus producing coordinated movements of the legs [4], [5]. In animal models, this technique has shown substantial promise for restoring standing and walking after SCI [1], [3], [6]–[8].

The ISMS implants used for restoring standing and stepping to date are comprised of 8–12 microwires individually implanted in each side of the spinal cord [6], [7], [9], [10]. The wires are manually positioned; thus, allowing for flexibility in placement within the cord. However, the process of inserting individual microwires can be tedious and may be susceptible to placement errors which can reduce the overall yield of the ISMS implant [9]. The use of arrays of electrodes that are held together by a base could improve the accuracy of tip placement in the ventral horn of the cord, while reducing the time of surgery. By adhering to the surface of the pia mater, the base will also increase the stability of the electrodes within the spinal cord. Currently available electrode arrays are capable of recording from or stimulating various regions of the brain. Examples of such arrays include the Utah, Michigan and Huntington Medical Research Institute (HMRI) arrays, all of which consist of arrangements of multiple electrodes that are held together by a rigid, glassy polymer or silicon base [11]–[14].

Studies have suggested that within the brain, mechanical mismatch between stiff electrodes and soft tissue can lead to adverse inflammatory responses [15], [16]. To address this issue, a number of electrode designs incorporating flexible polymers into the electrodes themselves have been implemented, ranging from multisite neural probes fabricated on polyimide substrates [17], [18], microthread electrodes based on organic materials [19], to mechanically adaptive cortical implants fabricated from polymer nanocomposites which undergo a dramatic change in modulus upon implantation as water is absorbed [20]. Each of these devices could potentially be utilized in the spinal cord as an independent unit, and a base would be advantageous to simplify the insertion process.

The mechanical properties of electrode arrays intended for use in the spinal cord must be carefully controlled. The spinal cord undergoes large deformations during daily motion (average maximal elongations of 10.1% were observed in human volunteers by MRI along the posterior side of the cervical side during flexion [21]), and arrays that are able to deform with the cord are needed. With the exception of the HMRI electrode arrays, a version of which has been implanted in the spinal cord [22], the interaction of the above mentioned arrays with spinal cord tissue as well as their long-term stability in the spinal cord remain unknown [23].

One approach to improving the mechanical properties of microelectrode arrays in vivo has been to engineer devices integrating biodegradable materials, which will be suitably stiff to manipulate and implant, but then gradually erode upon implantation, leaving only wires

[24], or micropatterned neural probes [18], [25]. However, this approach is not suitable for ISMS electrode arrays for two reasons: (1) Degradation needs to occur within a few hours of implantation, allowing the solid base to erode fully prior to the patient's commencement of movement following recovery from anesthesia. This ensures that the stiff base does not cause damage to the mobile cord. However, the solid base cannot erode too fast (as would be the case when utilizing sucrose-based approaches) such that contact with fluids during the implantation procedure dissolves the base prior to proper positioning within the cord. (2) For most materials, swelling is an integral part of the degradation process, which may disturb the electrodes themselves.

Therefore, we propose that a flexible base electrode array (FBEA) may be a suitable alternative for intraspinal microstimulation interfaces. During normal daily motion, the flexible base of the array would conform to the surface of the pia mater and undergo the same deformations as the cord. This in turn would allow the penetrating electrodes to "float" within the spinal cord tissue as it moves, thus providing enhanced interfacial stability. Devices with bases could also potentially be utilized to improve the longevity of recording in the central or peripheral nervous system. The base stiffness of currently available electrode arrays likely contributes to the inflammatory response, electrode encapsulation, and ultimately the failure of these devices [26].

The fabrication of an FBEA to interface with the spinal cord requires the development of a customizable protocol to accommodate for variations in curvature and size of the lumbosacral spinal cord between recipients of the device. Moreover, depending on the leg movements to be restored, the target regions for stimulation within the ventral horn could vary [4]. Unlike the brain, the ISMS interface does not require an array with a high density of electrodes [3], [8], [11]–[13]. Because the target locations for producing various synergistic movements are distributed along the rostrocaudal extent of the lumbosacral enlargement, an array with a sparse arrangement (instead of dense distribution) of electrodes along the length of the enlargement would be suitable for interfacing with the spinal cord [3], [8]. The relatively large length requires the use of a more flexible device than in applications where the target region is smaller in dimension. While various flexible arrays have been described previously in the literature [27]–[29], [21]–[23], the electrodes in these devices are patterned in the plane of the surface. For intraspinal microstimulation, protruding, high aspect ratio electrodes that can access the ventral horn region of the cord are required.

In this paper, we describe the development of a FBEA that could be used for ISMS. A fabrication protocol which enables customization of the array was developed. The devices were implanted into surrogate cords which mimicked the mechanical properties of the natural spinal cord [30], and the mechanical behavior of the implanted FBEAs under tension was assessed and compared to the behavior of implanted arrays of individual microwire without a base as well as arrays with rigid bases. Similar rigid base arrays have been successfully utilized previously for stimulation in the cat spinal cord in acute experiments; these arrays consist of iridium wires (75 μm diameter) in a rigid epoxy base [22]. Finally, a validated finite element model (FEM) of the surrogate spinal cord was used to analyze the stresses that various electrode array types impose on spinal cord tissue. When implanted in surrogate cords, FBEAs were able to undergo significantly higher deformations than rigid bases, comparable with the deformations achieved by individual microwires. The FEM also showed that the electrodes of the FBEA impose smaller stresses on the surrogate cord than the rigid arrays, yet somewhat higher stresses than the individual electrodes.

# II. Methods

## A. Array Fabrication

The flexible array consisted of a curved flexible base with two rows of protruding electrodes (30 μm wires each, 4 mm in length), as illustrated in Figure 1. Thin stainless steel wires with 30 μm diameter (insulated with 4 μm of polyimide) were selected in our design to minimize the overall stiffness of the base itself, as each lead and corresponding electrode was comprised of a continuous wire. The upper and lower surfaces of the base were designed with a curved profile to match the curvature of the spinal cord itself, as can be determined by magnetic resonance imaging (MRI) [9]. Employing a curved base is expected to increase the adherence of the array to the surface of the pia mater, and reduce the extent of connective tissue formation between the spinal cord and the base of the array, thus diminishing the chances of array dislodgement [31]. The thickness of the base of the array was a key design parameter. Ideally, this dimension should be minimized to enable the array to be implanted in the available space between the pia mater and dura mater surrounding the spinal cord. At the same time, the base should be thick enough to form a continuous layer around the leads connecting to the electrodes and to resist tearing during deformation. To engineer a base that can be tested in a feline model, a target thickness of 300 μm was selected. The shape of the base was controlled by curing the elastomer in a customized, rapid-prototyped mold, in which the electrode wires were placed. The elastomer was the biocompatible silicone ‘MED 6215’ (NuSil Technology, Carpinterial, California, USA). This was selected as the base material because silicone elastomers are commonly used in medical implants and neural interface applications [27], [32]–[36], and have moduli of elasticity (~1 MPa, *vide infra*) orders of magnitude smaller than that of other polymers such as polyimide (3.5 GPa [37]) and parylene (3.2 GPa [37]). MED 6215 was used as received, and prepared in the suggested elastomer to cross-linker mixing ratio of 10:1. Samples were cured for 60 minutes at temperatures of 66 °C. The design of the mold was prepared using 3D CAD software (Pro/Engineer Wildfire 3.0 (Parametric Technology Corporation, Needham, MA, USA). It consisted of two parts: 1) A female component (Figure 2a) which controlled the length and curvature of the base and the location of electrodes. The length and width of the base (2 cm and 0.7 cm, respectively) were determined by the closed back side of the mold, and the location of the electrodes was determined by the holes created in the mold (Figure 2a). The mold height was chosen to be larger than the maximal height (depth) of the electrodes, and various molds with a range of heights were constructed. Small holes were included in the female half of the mold, through which the electrodes could be inserted. 2) A male component (Figure 2b) controlled the thickness of the base and ensured that its thickness was uniform throughout its length by matching the curvature of the female mold. The mold had openings at both ends to facilitate solvent evaporation.

Rapid prototyping (3D printing) was used to fabricate transparent plaster molds with glossy smooth surfaces, using Objet FullCure720 (Objet Ltd, Billerica, MA, USA). A glossy surface was selected to weaken any potential bond between the silicone elastomer and the surface of the molds. The fabricated molds were cleaned first using a water jet. The pressure of the water removed all particles and resins that were attached to the surface. The molds were then placed in sodium hydroxide solution prepared by mixing 10 g of NaOH (Anachemia Canada Inc., Quebec, Canada) in 500 ml of distilled water. After 1 hour, the molds were removed, dried and cleaned again by a water jet. The dried molds were then silanized in a vacuum chamber dessicator, with a drop of trichloro(1,1,2,2-perfluorooctyl)silane. The silane layer was used to prevent the polymerized silicone elastomer from sticking to the surface of the molds. For base thicknesses of 300 μm, it was difficult to achieve full polymerization due to surface inhibition effects that became dominant as the separation between the molds was reduced. Therefore it was necessary to utilize a larger separation (398 um), lined on each side with a thin (49 um) layer of acrylic

adhesive-backed polypropylene (Tartan 3690 Clear Packaging Tape, 3M), as shown in Figures 2c and 2d. A thin hypodermic needle was used to puncture holes in the film that corresponded to the holes in the female part of the mold to facilitate the insertion of the electrodes through the holes in the liner.

Once the molds were prepared, the electrodes were inserted through customized positioning holes. The location of the electrodes in the array was determined by the location of small (235 um) holes in the mold through which the wires were fed prior to pouring in the monomer mixture composing the base. The location of these holes could be varied to match the location of the electrodes to the target regions within the ventral horn of the lumbosacral enlargement (as determined, for example, by MRI). Mushahwar et al. [4] mapped the approximate size and location of different motor neuron pools that innervate various muscle groups, and similar to earlier work [38]–[41], found that the different pools have different sizes and medio-lateral, dorso-ventral arrangements within the lumbosacral enlargement. Therefore, to activate different muscles and movement synergies, the electrodes within the array should reach the target motor neuron pools.

The electrodes themselves consisted of stainless steel microwires. In the literature, both Platinum/Iridium (Pt/Ir) and stainless steel (SS) microwires 30 μm in diameter [6]–[8], [42], as well as multi-contact microfabricated cylindrical electrodes 85 μm in diameter [32], [42], have been used for ISMS applications. For the present work, 30 μm SS wires (insulated with 4 μm of polyimide) were obtained from California Fine Wire (Grover Beach, California, USA). The microwires were bent to the desired height (depth) to form a continuous electrode-lead as described previously [6], [8]. After placement of the electrodes in the mold, the base precursor could be introduced into and set in the mold. A completed array is shown in Figure 3.

### B. Rapid Prototyped Handles

To facilitate the handling of the array and structural preservation during implantation, a temporary handle was adhered to the top of the flexible base.

Handles were designed in 3D CAD software and rapid prototyped. To adhere the handles to the bases, a photopolymerizable glue was prepared by mixing polyethylene glycol diacrylate (PEGDA, molecular weight 575, Sigma-Aldrich, Oakville, Ontario, Canada) with 0.5 wt % photoinitiator (CIBA Irgacure 651, BASF, Mississauga ON). The top surface of the silicone base was treated by UV ozone for 10 minutes to allow better adhesion to the PEGDA layer. A small drop of PEGDA was applied and the handle was positioned in place. The glue was then polymerized for 10 minutes by placing the base and handle approximately 5 cm away from an 8 W UV lamp at 365 nm.

### C. Tensile Testing

An Instron single column tabletop system with 1 kN load cell (Model 5943, Instron, Norwood, MA) was utilized to characterize the elastic modulus of the silicone base material, according to ASTM standard D412D, which is briefly summarized here. Samples were cured in dogbone-shaped Al molds (ASTM D412 type D, with a 3 mm x 3 mm x 32 mm testing range) for 90 minutes at 66°C. Samples were clamped using self-tightening roller grips (Instron 2713) and pre-loaded with 0.05 N of force to ensure that the samples were straight before deformation. They were then loaded at a rate of 50 mm/min until an elongation of 10 mm was reached. Assuming a Poisson’s ratio of 0.5 (for incompressible materials), Young’s modulus was calculated from the slope of the stress-strain curve between 1 mm and 2 mm of deformation.

### D. In vitro Testing: Elongation

To assess the mechanical compatibility of the FBEAs with the spinal cord, arrays with 2 rows of 4 electrodes with a diameter of 30 μm, and a base thickness of 300 μm embedded with straight lead wires (30 μm in diameter) were fabricated. The inter-row separation was 4 mm and inter-electrode spacing was 3 mm, resembling the average microwire separations utilized in ISMS implants [3]. The FBEAs were implanted into surrogate spinal cords designed to have mechanical properties (bulk modulus, surface frictional forces, dimensions) that mimic those of the actual human spinal cord [30]. These cords consisted of hydrated gelatin (12 wt% in water), which were crosslinked with a small amount of formaldehyde (19.4 mmol/100 ml solution), and molded in a cylindrical shape with elliptical cross-section (6 mm x 8 mm). These dimensions were selected to mimic those of an actual cat spinal cord. The cords were mounted in a Teflon stand (Figure 4a), and implanted with the desired electrode arrays. Beyond implantation, further steps to anchor the arrays to the surface of the cords were not taken, thus allowing the arrays to float freely within the cord. In in vivo settings, the arrays would be covered by a thin plastic film to prevent the adhesion of muscles and surrounding tissue. After implantation, the cords were subjected to 12% uniaxial tensile strain (midway between the average (10.1%) and maximum (13.6%) values described in the literature for the cervical spinal cord during flexion [21]). The results were then compared to those obtained in similar experiments conducted using: a) surrogate cords implanted with electrode arrays in which the electrodes (with 80 μm diameter) were joined by a rigid base; and b) surrogate cords with implanted electrode arrays comprised of individual microwires (30 μm diameter) without a base. Note that data for (a) were published previously in [30].

The same strain analysis technique reported in [30] was used. Briefly, reference dots were drawn on the surrogate cord (Figure 4b). At least three pictures were taken of the surrogate cords before and after the application of 12% strain using a Canon EOS 1000D (Canon Inc., Rockville, MD, USA). The distances between the reference dots were measured using Carl Zeiss AxiVision Rel. 4.6 software. The dimensions of the stand were used for calibration and conversion of measurements from pixels to millimeters.

### E. Finite Element Model

A two dimensional FEM was constructed using ANSYS 11 (ANSYS Inc, Canonsburg, PA, USA) to simulate the in vitro strain test and calculate the stresses experienced by the tissue around the implanted arrays. The dimensions and material properties of the surrogate cord and FBEAs were obtained from empirical measurements. FBEAs with eight (2×4) electrodes with diameters of 30 μm and heights of 4 mm, base thicknesses of 300 μm, 600 μm, and 1 mm, and a modulus of elasticity of 1000 kPa (based on tensile testing results) was modeled. The electrodes themselves were assumed to be in full contact (i.e., no slippage) with a cord of diameter 7.5 mm and length 40 mm, and to have a slanted tip. To best approximate the actual conditions encountered in our experiments, slippage was allowed between the surface of the array and the surface of the cord, and between the base and the electrodes themselves (due to imperfect bonding between the surface of the electrodes and the silicone base. This allowed the electrodes limited freedom both to travel laterally within the snuggly fitting channels that surround them in the base, and to rotate with respect to the substrate normal). The modulus of elasticity of the cord (without pia mater and dura mater) was assumed to be 90 kPa [34]. An eight node quadrilateral element with two degrees of freedom was used to mesh the model. The cord and the silicone elastomer base were assumed to operate in the elastic range and static analysis was performed.

A 12% uniaxial tension was evenly distributed between the left and right boundaries of the cord. The location of the nodes in the model coincided with the actual location of the

reference dots drawn on the cord in the experimental work. The distance between the nodes was measured before and after the application of the 12% deformation and strains were calculated. The results obtained from the model were validated against the experimental results obtained for the cords implanted with flexible and rigid base arrays. In the model, the rigid base array was simulated by increasing the modulus of elasticity of the base to 1 GPa.

The validated model was then used to study the effective (Von Mises) stresses applied by the electrodes on the spinal cord tissue. To decrease the effect of singularities at the electrode tips, the stress values were measured and plotted for a region 10 μm away from the interfacial layer between the electrode and the surrounding medium. The distance was chosen so that the obtained stresses were within the set of elements interfacing the electrodes and the spinal cord. The model assumed that the spinal cord was isotropic, and contained no hydrostatic pressures. Simulations of implanted cords with 12% uniaxial tension (applied from one end while the other end remained fixed) were then performed and the stresses induced by the electrodes of flexible arrays, rigid arrays and arrays without bases were examined. Due to the symmetry of model geometry, stresses caused by the 2 outer electrodes (1 and 4) were assumed to be similar; so were the stresses applied to the 2 inner electrodes (2 and 3). Therefore, the stresses due to 1 outer and 1 inner electrode are presented.

## III. Results

### A. Tensile Testing

The FBEA consisted of three main parts: the base, the electrodes and the lead wires. For ISMS applications, the base of the array needs to have the same curvature and stiffness of that of the spinal cord. Moreover, customizable electrode spacing and adequate stress-relief in the lead wires are needed. The Young's modulus of MED 6215 – the elastomer used to fabricate the bases of the array – was measured to be 1.06 ± 0.14 MPa. This value is considered acceptable as it is within the range of moduli measured for human cervical and thoracic spinal cord tissue with pia mater characterized in vitro under tension, for strains of 9% (1.2 ± 0.5 MPa) [35]. The measured value (1.06 ± 0.14 MPa) was utilized in the FEM, and to calculated the stiffness ($K$) of the base (0.105 N/mm), using the equation $K=EA/L$ (approximating the array as a beam with a flat rectangular cross-section rather than a curved one).

### B. In Vitro Testing: Elongation

The surrogate cord with the implanted FBEAs was subjected to 12% axial strain and the distances between reference marks on the cord (Figure 4b) were optically measured before and after the application of strain. The results were compared to those obtained by Cheng et al. [30] for surrogate cords implanted with electrode arrays in which the electrodes were held by a rigid base; and surrogate cords with implanted individual, 30 μm stainless steel electrodes. The rigid base arrays and the individual electrodes had the same electrode layout as the FBEAs in this study.

Surrogate cords implanted with FBEAs showed deformations that were very similar to those implanted with individual microwires (Figure 5). The strains measured between the reference points in the surrogate cord implanted with the FBEAs ranged between 9 ± 2% to 12 ± 1% which was within the range of uncertainty for the strain values obtained for the individual microwires (10 ± 2 % to 12 ± 1%).

The strains measured in cords implanted with FBEAs were significantly different from those measured in cords implanted with rigid base arrays. The strains observed in the rigid base arrays were particularly low in the region located beneath the electrode array itself (Figure

5): the strain values associated with L1 and L2 were only 3 ± 1% and 5 ± 1% respectively. As the reference lengths along longer sections of cord are considered, these values increased to 8 ±1% and 9 ± 1%, respectively.

### C. Finite Element Model

**1) Model Validation—**The calculated strains in the numerical model of the cords implanted with FBEAs and rigid base arrays were plotted against the empirical measurements obtained from the physical model (Figure 5). For the cords implanted with the FBEAs, the strains calculated along all reference lines (L1 through L4) in the numerical model were within the standard deviations of the respective strains in the physical model. Similar results were observed for the rigid base arrays, although the value predicted by the FEM model for the strain along line L3 was slightly more than one standard deviation below the average value seen experimentally (1.1 standard deviations lower), and the difference between the calculated value of L4 and the average experimental value was 1.84 times the standard deviation. In both cases, these values are therefore within the 95% confidence interval (i.e. within 2 standard deviations). The results obtained numerically were therefore in good agreement with the models.

**2) Stresses Induced by the Arrays—**The validated numerical model was used to calculate the stresses induced by the electrodes of various types of arrays on the surrounding spinal cord tissue. Cords implanted with individual wires were modeled by allowing electrodes to move freely with the cord. This simulation was based on the assumption that no external forces are transferred to the individual electrodes by the lead wires which connect to the power supply (ideal case). The calculated stresses induced by electrodes in arrays with individual wires, flexible base and rigid base arrays on spinal cord tissue are shown in (Figure 6). The stress induced by electrodes in all array types was highest at the interfacing edge with the cord (distance from interfacing edge = 0), decreased exponentially along the length of the electrode and increased again around the tip. The spike in stress at the tip occurs because of the discontinuity in materials at this point, while the higher value at the surface results from the boundary conditions at this interface which constrain the deformation of the wire and lead to higher stress. The magnitude of the stresses induced by the electrodes differed between the three different arrays. The stress magnitudes on the surrounding tissue induced by the outer and inner electrodes in the arrays without a base were nearly identical; however, substantial differences between the stresses induced by the outer and inner electrodes were seen in the flexible and rigid base arrays. The outer electrodes in the arrays comprised of individual 30 μm wires induced a stress of 36.6 kPa and 26.8 kPa at the top and tip, respectively (Figure 6a); while the inner electrodes induced 35.2 kPa and 26.0 kPa at the top and tip (Figure 6b). In contrast, the outer electrodes in the rigid base array induced much higher stress at the top (66.3 kPa) than in the individual wires, but lower stress at the tip (20.6 kPa) (Figure 6a). Meanwhile the inner electrodes in the rigid base array induced lower stresses than for the individual wires (20.0 kPa and 19.1 kPa) (Figure 6b). These results show that in the individual wires, stress at the interface between the electrodes and the tissue is more evenly distributed throughout the device, while in the rigid base array, stress is more highly concentrated on the outer electrodes, particularly at the top. The stresses induced by the 300 μm thick FBEA fell in between those induced by the arrays without bases and the rigid base arrays. The outer electrodes induced a stress of 50.4 kPa at the top and 22.5 kPa at the tip (Figure 6a) while the inner electrodes induced 30.2 kPa and 25.6 kPa at the top and tip, respectively (Figure 6b). As the base thickness was increased to 1 mm, the stress at the top of the outer electrodes (66.8 kPa) increased towards the value seen for the 1 mm thick rigid base array (66.3 kPa). This trend is due to the fact the base thickness has a significant effect on the value of the base stiffness, and can raise the stress concentration close to the base, particularly at the outer electrodes. In

contrast, the stress at the tips was slightly less than for the rigid base (17.8 kPa compared with 20.6 kPa). To verify that the higher stresses observed for the rigid base arrays were due to properties of the base and not the dimensions of the electrodes themselves (75 μm vs. 30 μm), this value was also utilized in the model. Significant differences were not observed (results not shown).

The ratio of stresses induced by the outer to inner electrodes, from the surface of the spinal cord to 1 mm below the tip of the electrodes, for the various electrode arrays is shown in Figure 6c. The ratio of induced stresses by the outer to inner electrodes in the rigid base array was 3.3:1 and 1.1:1 at the top and tip, respectively. This ratio was 1.7:1 and 0.9:1 for the 300 μm FBEA and 1.0:1 and 1.0:1 for the arrays without bases.

## IV. DISCUSSION

### A. Overview

The goal of the present work was to develop a customizable, rapid fabrication process for a multi-electrode array for ISMS applications. Such an array could facilitate the implantation procedure and increase the targeting accuracy of the electrodes. Most of the currently available arrays are rigid and have been developed to interface with the brain [11]–[14], [31]. Due to the small size of the arrays relative to the brain, the imposed mechanical and geometrical constraints on the interfacing rigid arrays may not be significant. In contrast to existing systems, ISMS implants for restoring standing and walking require low density electrodes that span 3–5 cm of the spinal cord. Therefore, the region of the implant undergoes relatively more pronounced deformations during natural movements and requires that arrays implanted within the spinal cord possess mechanical properties that are compatible with the tissue. In this study, we fabricated several FBEAs and characterized the developed prototypes. The design was modified to produce the maximal mechanical compliance between the array and the human spinal cord. The prototypes were then implanted in surrogate cords and subjected to uniaxial strain tests that mimicked the highest strain experienced by the human cord during daily motion.

### B. Mechanical Compatibility of the Implanted Array and the Spinal Cord

Previous in vitro testing suggested that the mechanical compliance between the surrogate spinal cord and the implanted arrays significantly influences the mechanical behavior of the cord [30]. Rigid base arrays in particular impeded the motion of the cords when elongated. Rousche et al. [29] proposed flexible base intracortical arrays which consisted of polyimide base and electrodes. The polyimide layers had a modulus of elasticity of ~3 GPa which is more than 3 orders of magnitude larger than that of the spinal cord. Thus, it was important to develop a new type of compliant array with a stiffness that matches that of the spinal cord. In this study, a soft, biocompatible silicone elastomer was used as the base material.

### C. Cords Implanted with FBEAs Undergo Similar Deformations as Cords Implanted with Individual Microwires

The spinal cord undergoes three types of deformations during daily movements: elongation, torsion and flexion. These deformations have been quantified [35], and a maximal strain of 13.6% of the posterior surface during flexion was reported, where the average value seen across the 5 study participants was 10.1%. To our knowledge, similar studies have not been performed in people with spinal cord injury; therefore, the elongation (12%) used in this study was selected based on the average value observed in un-injured individuals. We have previously presented a methodology to assess the influence of implanted arrays on the mechanical behavior of the spinal cord [30]. The methodology studied the behavior of surrogate cords elongated by 12% when implanted with rigid base arrays, and arrays

comprised of individual microwires without a base. We showed that the rigid base arrays impede the motion of the cord, while individual wires move with the cord without significantly affecting its mechanical behavior. We hypothesize that the impediment of motion caused by the rigid base arrays may cause physical damage to the cord if chronically implanted. In the study presented here, the influence of our newly-developed FBEA on the surrogate spinal cord was assessed using the same method. The strains observed in surrogate spinal cords implanted with FBEAs were similar to those measured for the cords implanted with individual wires (Figure 5). The similarity in strain to individual wires suggests that the FBEAs may be mechanically compatible with the cord and that they could be well tolerated by the spinal cord in this regard if chronically implanted [42].

### D. Stresses Induced by Electrodes in the FBEA on Surrounding Tissue

The finite element model served as an important tool to further understand the mechanical interaction between the electrodes of different types of arrays and the spinal cord. To validate the model, the strain behavior of cords implanted with various types of arrays was evaluated, and compared with the experimental results. Good agreement between the experimental data and the model was seen, as shown in Figure 5. This validated model is an important tool that can be used to quickly assess how various design parameters (such as base thickness, electrode diameter, etc.) affect the mechanical behavior of a spinal cord into which the array is implanted. Furthermore, the model allowed for a comparison of the stresses imposed by the electrodes of the FBEAs (with calculated base stiffness of ~ 0.105N/mm) and rigid-base arrays (with calculated base stiffness of ~ 350 N/mm for a device with the same dimensions, i.e. 2 cm long, 0.7 cm wide, and 1 mm thick) on the cord to those induced by arrays of individual microwires currently used in ISMS implants [3], [9], [10], [42].

The stresses were maximal at the interfacing layer between the base and the cord (Figure 6) due to the mismatch in the stiffness between the base, the electrode and the spinal cord. The increase in the stress at the tip was largely due to the discontinuities caused by the sharp edge of the tip [43]. The inner and outer electrodes in arrays of individual microwires without a base induced similar stresses against the cord, giving an approximately uniform stress ratio of 1 (Figure 6). This is due to the similarity of deformations across the cords implanted with no-base arrays; i.e., the electrodes moved freely with respect to each other due to the absence of any base. The outer electrodes exerted twice as much stress at the interfacing edge relative to the inner electrodes in the FBEAs; while the outer electrodes exerted 3 times more stress than the inner electrodes in the solid-based arrays. This effect is referred to as “stress shielding”, where an entity, such as the outer electrodes, in the loaded domain will bear the majority of the stress applied on the domain and shield other entities, such as the inner electrodes in its shadow, from most of the stress. The stress shielding induced by the outer electrodes, especially in the solid-based arrays, corresponds to the smaller deformation and lower strain values measured at L1 relative to L2 (Figure 5). The higher strains/stresses around the outer electrodes in the solid-based arrays indicate that more tissue damage could be induced at these locations if the arrays were to be implanted in vivo. The substantially smaller stress shielding caused by the outer electrodes in FBEAs would likely produce much less pronounced tissue damage. Nonetheless, the best case, which is that of individual wires, showed almost no shielding. Arrays of individual wires correspondingly were well tolerated by the spinal cord and caused minimal tissue damage when implanted chronically in cats and rats [9], [10], [42]. Therefore, to ensure higher mechanical compliance between the FBEA and the spinal cord, the stiffness of the flexible base should be further decreased by decreasing its thickness and modulus of elasticity.

### E. Study Limitations

The two-dimensional FEM used in this study considered the spinal cord an isotropic medium. The spinal cord is an anisotropic structure that allows for unique electrochemical and electrophysiological functions. Nonetheless, for mechanical testing of indwelling electrodes, the isotropic structure with a modulus of elasticity that matches that of the human spinal cord provided an acceptable medium for assessment of tensile deformations. The models also did not take into account the change in material properties of the cord immediately post implantation. The natural immune response to implanted foreign bodies will initiate a cascade of reactions leading to initial swelling (increased stiffness of the spinal cord) and ending with fibrous encapsulation of both the implanted electrodes.

While the present model was executed in two dimensions, we believe that it sufficiently describes the system, since there are no forces or constraints within the third (omitted) dimension that should influence the electrodes (provided that the spacing between the adjacent rows of electrodes is sufficiently large). This is a special case 3D case known as a plane strain condition. Nonetheless, an explicitly three-dimensional model could potentially be utilized in the future to present a more complete map of the stress profiles around the electrodes.

### F. Future Work

Development of the FBEAs is ongoing. While the flexible base arrays presented in this study had straight leads that were embedded in the base, future arrays will include embedded coiled leads. The lead material and coiling will be chosen to have a modulus of elasticity similar to that of the flexible base for an elongation that matches that experienced by the spinal cord during natural movement.

To enable the array to be utilized in a clinical setting, the mechanism and integrity of all connections must be optimized to prevent failure of the devices at these points.

While the surrogate cord has been a useful tool for preliminary studies, studies in an animal model are critical to ensure that similar behavior is observed under deformation, and also to verify that the electrodes can be inserted without deforming or buckling. Experiments in an animal model will also enable the development of a suitable insertion protocol. Additionally, histological assessments of arrays implanted chronically in vivo will be conducted.

## V. CONCLUSION

The current work presents the first study to assemble microwire electrodes into a flexible base array. It is also the first to assess the influence of these arrays on the mechanical behavior of surrogate spinal cords. A feasible, customizable fabrication process for such arrays was presented. The flexibility of the design allows for variations in the curvature and geometry of the base. The density and location of the electrodes can also vary.

The high flexibility of the developed design makes it an ideal candidate to interface with other neural systems, such as the brain or dorsal root ganglia. The arrays will be modified to match the curvature of the targeted system to ensure full contact between both surfaces. The mechanical properties of the array will also be tuned to match the target stiffness resulting in maximal mechanical compliance between the two interfacing media. The fabrication protocol also allows for the use of different kinds and densities of electrodes depending on the targeted neural tissue.

## Acknowledgments

The authors acknowledge Dr. Kathryn Todd and Ms. Kimberly Paw for providing critical advice regarding the likely histological consequences of various electrode array properties, and Mr. Kian Parseyan for preparing and photographing the array shown in Figure 3. Funding for this work was provided by the Alberta Innovates – Health Solutions (AIHS), Alberta Heritage Foundation for Medical Research (AHFMR) and the National Institutes of Health (NIH). The tensile tester was purchased through the Canada Foundation for Innovation (CFI) Leaders Opportunity Fund. VKM is an AHFMR Senior Scholar.

## References

1. Mushahwar VK, Horch KW. Proposed specifications for a lumbar spinal cord electrode array for control of lower extremities in paraplegia. IEEE Trans Rehabil Eng. Sep.1997 :237–243. [PubMed: 9292289]
2. Hunter J, Ashby P. Secondary changes in segmental neurons below a spinal cord lesion in man. Phys Med Rehabil. Nov.1984 :702–705.
3. Mushahwar VK, Jacobs PL, Normann RA, Triolo RJ, Kleitman N. New functional electrical stimulation approaches to standing and walking. J Neural Eng. Sep.2007 :S181–S197. [PubMed: 17873417]
4. Mushahwar VK, Horch KW. Selective activation of muscle groups in the feline hindlimb through electrical microstimulation of the ventral lumbo-sacral spinal cord. Mar.2000 :11–21.
5. Mushahwar VK, Gillard DM, Gauthier MJ, Prochazka A. Intraspinal micro stimulation generates locomotor-like and feedback-controlled movements. IEEE Trans Neural Syst Rehabil Eng. Mar. 2002 :68–81. [PubMed: 12173741]
6. Saigal R, Renzi C, Mushahwar VK. Intraspinal Microstimulation Generates Functional Movements After Spinal-Cord Injury. IEEE Trans Neural Syst Rehabil Eng. Dec.2004 :430–440. [PubMed: 15614999]
7. Lau B, Guevremont L, Mushahwar VK. Strategies for generating prolonged functional standing using intramuscular stimulation or intraspinal microstimulation. IEEE Trans Neural Syst Rehabil Eng. Jun.2007 :273–285. [PubMed: 17601198]
8. Mushahwar VK, Collins DF, Prochazka A. Spinal Cord Microstimulation Generates Functional Limb Movements in Chronically Implanted Cats. Exp Neurol. Jun.2000 :422–429. [PubMed: 10833317]
9. Bamford JA, Mushahwar VK. Intraspinal microstimulation for the recovery of function following spinal cord injury. Prog Brain Res. 2011:227–239. [PubMed: 21867807]
10. Guevremont, L.; Mushahwar, VK. Neural Engineering: Research, Industry, and the Clinical Perspective. CRC Press; 2008. Tapping into the Spinal Cord for Restoring Motor Function after Spinal Cord Injury; p. 19-26.
11. Campbell PK, Jones KE, Huber RJ, Horch KW, Normann RA. A silicon-based, three-dimensional neural interface: manufacturing processes for an intracortical electrode array. IEEE Trans Biomed Eng. 1991:758–768. [PubMed: 1937509]
12. Maynard EM, Nordhausen CT, Normann RA. The Utah Intracortical Electrode Array: A recording structure for potential brain-computer interfaces. Electroencephalogr Clin Neurophysiol. Mar. 1997 :228–239. [PubMed: 9129578]
13. Hoogerwerf AC, Wise KD. A three-dimensional microelectrode array for chronic neural recording. IEEE Trans Biomed Eng. Dec.1994 :1136–1146. [PubMed: 7851915]
14. McCreery D, Lossinsky A, Pikov V, Liu X. Microelectrode array for chronic deep-brain microstimulation and recording. IEEE Trans Biomed Eng. Apr.2006 :726–737. [PubMed: 16602580]
15. Polikov VS, Tresco PA, Reichert WM. Response of brain tissue to chronically implanted neural electrodes. J of Neurosci Methods. Oct; 2005 148(1):1–18. [PubMed: 16198003]
16. Harris JP, Hess AE, Rowan SJ, Weder C, Zorman CA, Tyler DJ, Capadona JR. In vivo deployment of mechanically adaptive nanocomposites for intracortical microelectrodes. J Neural Eng. Aug. 2011 8(4):046010. [PubMed: 21654037]

17. Tooker A, Tolosa V, Shah KG, Sheth H, Felix S, Delima T, Pannu S. Optimization of multi-layer metal neural probe design. Conf Proc IEEE Eng Med Biol Soc. 2012; 2012:5995–5998. [PubMed: 23367295]
18. Wu, F.; Im, M.; Yoon, E. A flexible fish-bone-shaped neural probe strengthened by biodegradable silk coating for enhanced biocompatibility. Solid-State Sensors, Actuators and Microsystems Conference (TRANSDUCERS), 2011 16th International; 2011. p. 966-969.
19. Kozai TDY, Langhals NB, Patel PR, Deng X, Zhang H, Smith KL, Lahann J, Kotov NA, Kipke DR. Ultrasmall implantable composite microelectrodes with bioactive surfaces for chronic neural interfaces. Nat Mater. Dec; 2012 11(12):1065–1073. [PubMed: 23142839]
20. Harris JP, Capadona JR, Miller RH, Healy BC, Shanmuganathan K, Rowan SJ, Weder C, Tyler DJ. Mechanically adaptive intracortical implants improve the proximity of neuronal cell bodies. J Neural Eng. Dec.2011 8(6):066011. [PubMed: 22049097]
21. Yuan Q, Dougherty L, Margulies SS. In vivo human cervical spinal cord deformation and displacement in flexion. Spine. Aug; 1998 23(15):1677–1683. [PubMed: 9704375]
22. McCreery D, Pikov V, Lossinsky A, Bullara L, Agnew W. Arrays for chronic functional microstimulation of the lumbosacral spinal cord. IEEE Trans Neural Syst Rehabil Eng. Jun.2004 : 195–207. [PubMed: 15218934]
23. Harrison DE, Cailliet R, Harrison DD, Troyanovich SJ, Harrison SO. A review of biomechanics of the central nervous system--Part II: Spinal cord strains from postural loads. J Manipulative Physiol Ther. Jun.1999 :322–332. [PubMed: 10395435]
24. Gilgunn, PJ.; Khilwani, R.; Kozai, TDY.; Weber, DJ.; Cui, XT.; Erdos, G.; Ozdoganlar, OB.; Fedder, GK. An ultra-compliant, scalable neural probe with molded biodissolvable delivery vehicle. 2012 IEEE 25th International Conference on Micro Electro Mechanical Systems (MEMS); 2012. p. 56-59.
25. Lewitus D, Vogelstein RJ, Zhen G, Choi Y-S, Kohn J, Harshbarger S, Jia X. Designing Tyrosine-Derived Polycarbonate Polymers for Biodegradable Regenerative Type Neural Interface Capable of Neural Recording. IEEE Trans Neural Syst Rehabil Eng. Apr; 2011 19(2):204–212. [PubMed: 21147598]
26. Biran R, Martin DC, Tresco PA. The brain tissue response to implanted silicon microelectrode arrays is increased when the device is tethered to the skull. J Biomed Mater Res A. Jul; 2007 82(1):169–178. [PubMed: 17266019]
27. Meacham KW, Giuly RJ, Guo L, Hochman S, DeWeerth SP. A lithographically-patterned, elastic multi-electrode array for surface stimulation of the spinal cord. Biomed Microdevices. Oct.2007 : 259–269.
28. Meacham KW, Hochman S. Selective stimulation of the spinal cord surface using a stretchable microelectrode array. 2011; 5
29. Rousche PJ, Pellinen DS, Pivin DP, Williams JC, Vetter RJ, Kirke DR. Flexible polyimide-based intracortical electrode arrays with bioactive capability. IEEE Trans Biomed Eng. 2001:361– 371. [PubMed: 11327505]
30. Cheng C, Kmech J, Mushahwar VK, Elias AL. Development of Surrogate Spinal Cords for the Evaluation of Electrode Arrays Used in Intraspinal Implants. IEEE Trans Biomed Eng. 2013; 60(6):1667–1676. [PubMed: 23358939]
31. Rousche PJ, Normann RA. Chronic recording capability of the Utah Intracortical Electrode Array in cat sensory cortex. J of Neurosci Methods. Jul.1998 :1–15. [PubMed: 10223510]
32. Snow S, Jacobsen SC, Wells DL, Horch KW. Microfabricated cylindrical multielectrodes for neural stimulation. IEEE Trans Biomed Eng. Feb.2006 :320–326. [PubMed: 16485761]
33. Snow S, Horch KW, Mushahwar VK. Intraspinal Microstimulation using Cylindrical Multielectrodes. IEEE Trans Biomed Eng. Feb.2006 :311–319. [PubMed: 16485760]
34. Mazuchowski, EL.; Thibault, LE. Biomechanical Properties of the Human Spinal Cord and Pia Mater. presented at the Summer Bioengineering Conference, Sonesta Beach Resort in Key Biscayne; Florida. 2003. p. 1205p. 1206
35. Bilston LE, Thibault LE. The mechanical properties of the human cervical spinal cord in vitro. Ann Biomed Eng. Feb; 1996 24(1):67–74. [PubMed: 8669719]

36. Margulies, SS.; Meaney, DF.; Bilston, LB.; Thibault, LE.; Campeau, NG.; Riederer, SJ. In Vivo Motion of the Human Cervical Spinal Cord in Extension and Flexion. Proceedings of International IRCOBI Conference on the Biomechanics of Impacts; VERONA, ITALY. 1992.

37. Noh H, Moon K, Cannon A, Hesketh PJ, Wong CP. Wafer bonding using microwave heating of parylene intermediate layers. J Micromech Microeng. Apr.2004 14(4):625.

38. Vanderhorst VG, Holstege G. Organization of lumbosacral motoneuronal cell groups innervating hindlimb, pelvic floor, and axial muscles in the cat. J Comp Neurol. May.1997 :46–76. [PubMed: 9136811]

39. Romanes GJ. The motor cell columns of the lumbo sacral spinal cord of the cat. J Comp Neurol. Apr.1951 :313–363. [PubMed: 14832391]

40. Burke RE, Strick PL, Kanda K, Kim CC, Walmsley B. Anatomy of medial gastrocnemius and soleus motor nuclei in cat spinal cord. J Neurophysiol. May.1977 :667–680. [PubMed: 874534]

41. Van Buren JM, Frank K. Correlation between the morphology and potential field of a spinal motor nucleus in the cat. Electroencephalogr Clin Neurophysiol. Aug.1965 :112–126. [PubMed: 4157584]

42. Bamford JA, Todd KG, Mushahwar VK. The effects of intraspinal microstimulation on spinal cord tissue in the rat. Jul.2010 :5552– 5563.

43. Subbaroyan J, Martin DC, Kipke DR. A finite-element model of the mechanical effects of implantable microelectrodes in the cerebral cortex. J Neural Eng. Dec.2005 :103–113. [PubMed: 16317234]

## Biographies

**Imad Khaled** received the B.E. degree in mechanical engineering from the American University of Beirut, Lebanon in 2009 and the M.Sc. degree in mechanical engineering from the University of Alberta, Edmonton, AB, Canada in 2011.

**Cheng Cheng** received the exchange certificate in mechanical engineering from the Hong Kong Polytechnic University, Hong Kong, in 2008, the B.Sc. degree in materials engineering from Shandong University, Shandong, China, in 2009, and the M.Sc. degree in materials engineering from the University of Alberta, Edmonton, AB, Canada, in 2012.

**Salma Elmallah** is an undergraduate electrical engineering student at the University of Alberta, Edmonton, AB, Canada. In 2012, she worked with the Alberta Innovates-Health Solutions Interdisciplinary Team in Smart Neural Prostheses under the supervision of Dr. Elias in the Department of Chemical and Materials Engineering.

**Walied A. Moussa** received the B.Sc. and M.Sc. degrees from the American University of Cairo, Cairo, Egypt, in 1991 and 1993, respectively, and the Ph.D. degree from Carleton University, Ottawa, Canada, in 2000.

Currently, he is a Professor at the University of Alberta, with co-appointment to the Mechanical Engineering, Biomedical Engineering, and the Department of Surgery. His current research interests and publication of more than 100 articles are in MEMS and NEMS research and development in the biomedical, aerospace, mechanical, and environmental fields. His research work involves both experimental and numerical approaches to this field.

Dr. Moussa has Chaired the International Conference on MEMS, NEMS and Smart Systems (ICMENS) from 2003 to 2006 and is on the editorial board of a number of related journals.

**Vivian K. Mushahwar** (M’97) received the B.S. degree in electrical engineering from Brigham Young University, Provo, UT, USA, in 1991, and the Ph.D. degree in bioengineering from the University of Utah, Salt Lake City, UT, in 1996.

She was a Postdoctoral Researcher at Emory University, Atlanta, GA, USA, and the University of Alberta, Edmonton, AB, Canada. She is currently an Associate Professor in the Centre for Neuroscience, University of Alberta. Her research interests include identification of spinal cord systems involved in locomotion, development of spinal-cord-based neuroprostheses, incorporation of motor control concepts in functional electrical

stimulation applications, and development of systems for alleviating secondary side effects of immobility such as pressure ulcers.

Dr. Mushahwar is a member of the International Functional Electrical Stimulation Society, the New York Academy of Sciences, the American Physiological Society, the International Society for Magnetic Resonance in Medicine, and the Society for Neuroscience. She is also an Alberta Heritage Foundation for Medical Research Senior Scholar.

**Anastasia L. Elias** received the B.Sc. degree in engineering physics and the Ph.D. degree from the University of Alberta, Edmonton, AB, Canada, in 2002 and 2007, respectively. From 2003 to 2006, she was a Visiting Researcher at the Technische Universiteit Eindhoven, Eindhoven, The Netherlands. Since 2007, she has been a Visiting Worker at the National Research Council National Institute for Nanotechnology.

She is currently an Assistant Professor in the Department of Chemical and Materials Engineering, University of Alberta. Her research interest include designing and fabricating biocompatible electrode arrays for implantation, developing new techniques for shaping materials on the micro- and nanoscale, and engineering smart materials.

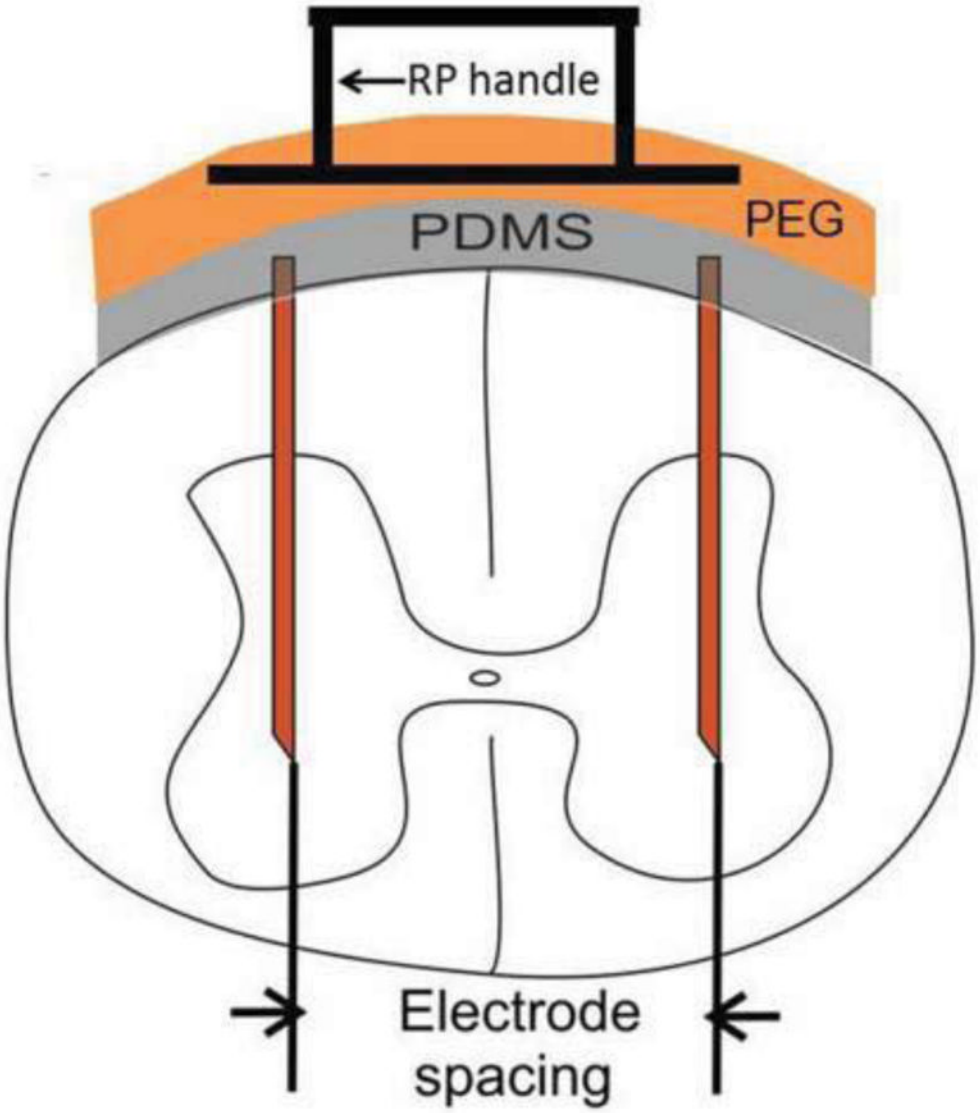


**Fig. 1.**
Schematic of the flexible electrode array. The array is shown implanted in the spinal cord with rapid prototyped handle to facilitate insertion (plan view).

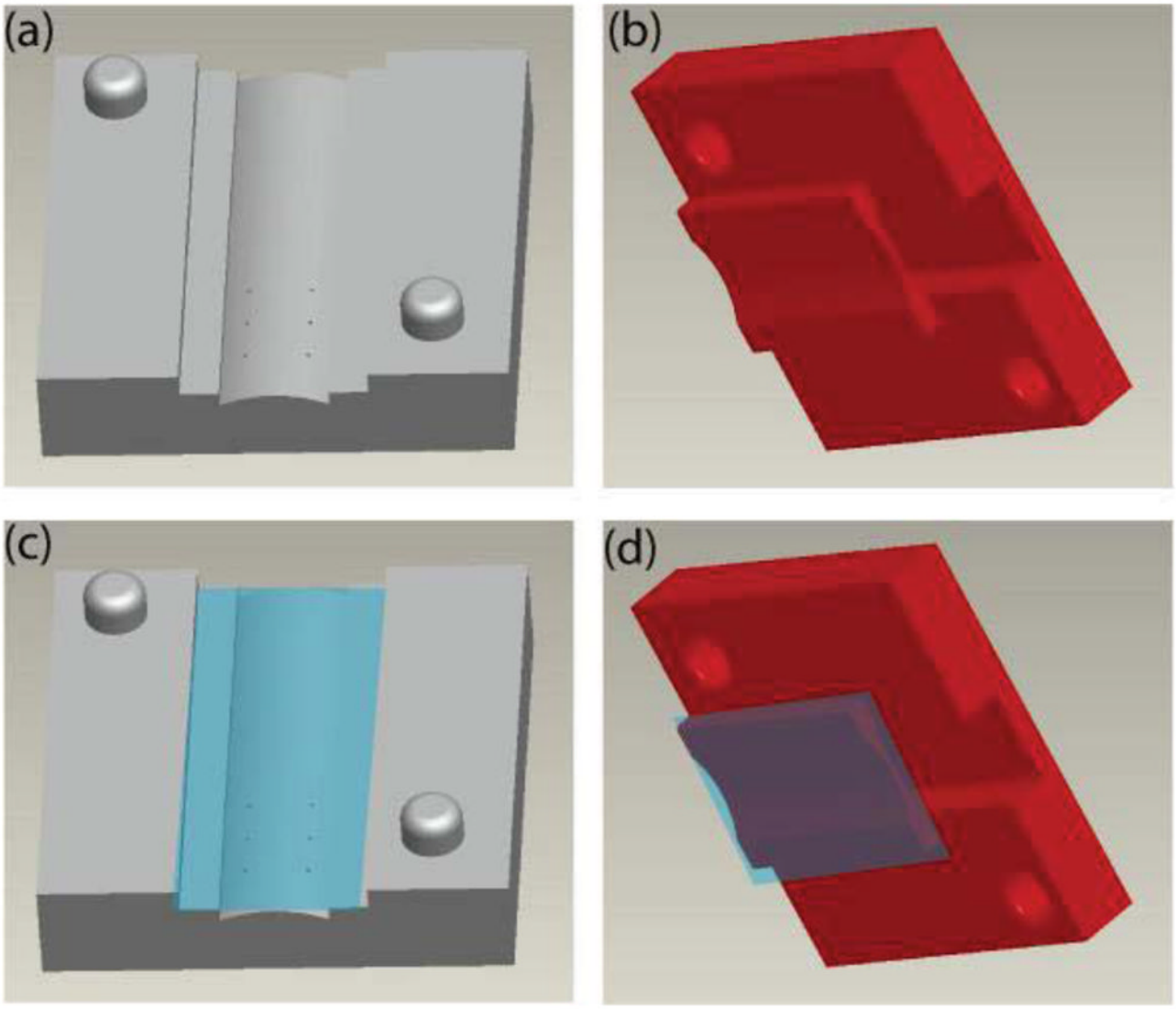


**Fig. 2.**

Rapid prototype mold and liner. CAD drawings of the female (a) and male components (b) of the molds are shown. The female component includes an array of six holes, through which the wires of the electrodes can be fed.

When working with thin layers of silicone elastomer, it was necessary to line the mold with a thin piece of polypropylene to ensure that polymerization would occur, as shown in (c, d).

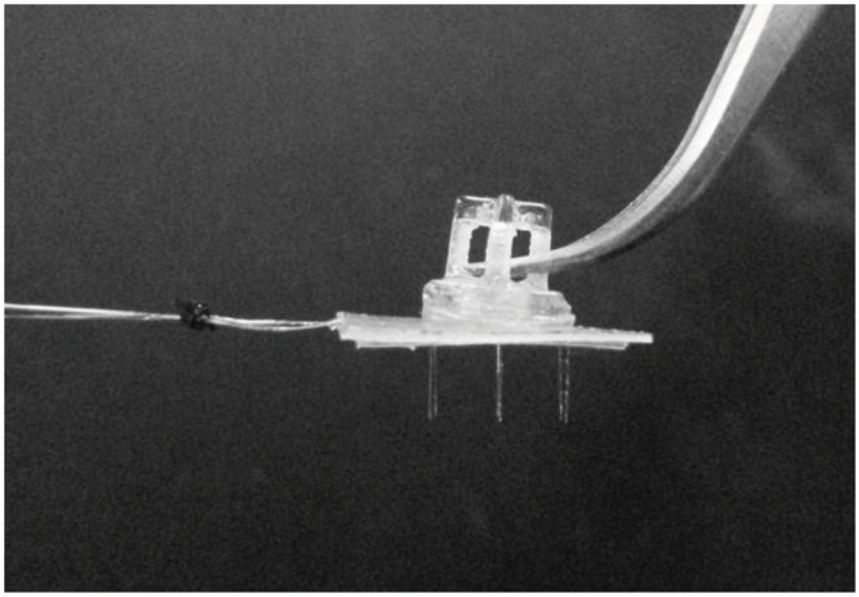

**Fig. 3.**
FBEAs. The flexible base electrode array, with rapid-prototyped handle. The handle was used to increase the stiffness of the flexible base temporarily. This improved the ease of handling and preserved the structural integrity of the array during implantation.

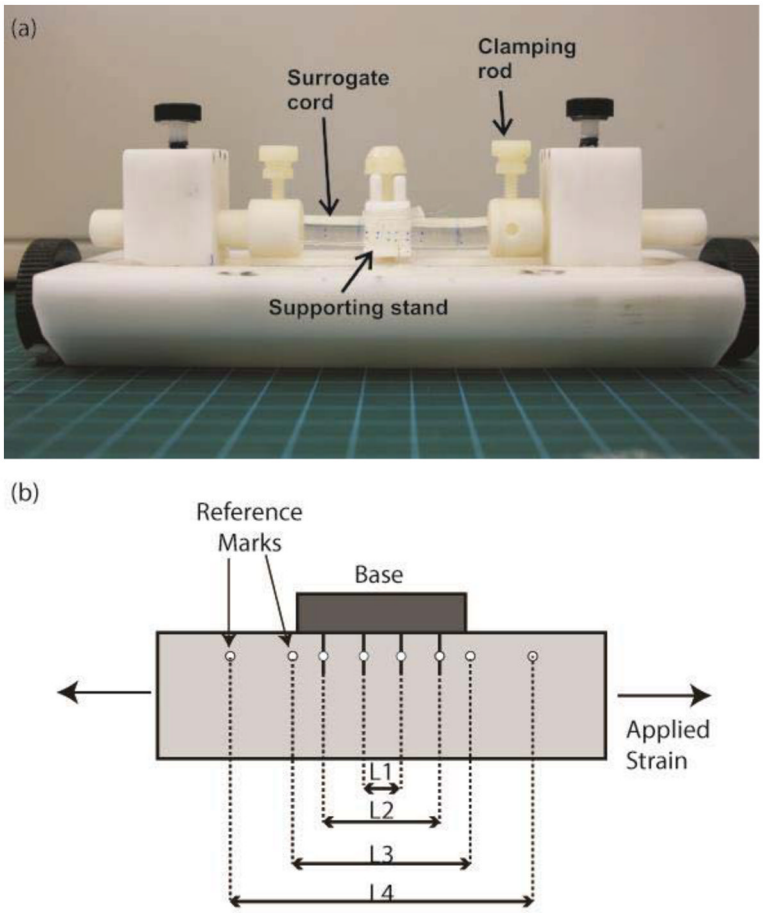


**Fig. 4. In-vitro testing of FBEAs**

Surrogate cord mounted in a teflon stand for empirical testing of mechanical compatibility of FBEAs (a), and schematic illustrating the markings used for measurements (b). Two rows of reference dots placed on the surrogate cord (upper and lower) were used to assess the interaction between the array and the cord. Strain values were measured between the different reference dots (L1 – L4) after the surrogate cord, implanted with various types of electrode arrays, was elongated by 12%.

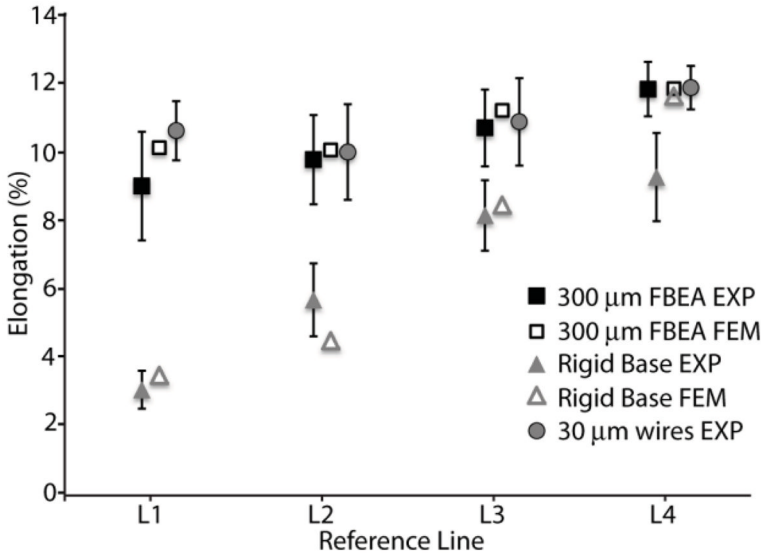


**Fig. 5. In-vitro testing and modeling of various electrode arrays**

Experimental results for the strain observed along reference lines L1, L2, L3 and L4 are shown for 300 μm FBEAs (filled squares), rigid base arrays (filled triangles) and arrays comprised of 30 μm stainless steel microwires. Finite element results for 300 μm FBEAs (open squares) and rigid base arrays (open triangles) are also shown. The data for the rigid base arrays (experimental) are reproduced from [30]. For experimental values, average values and standard deviations are shown.

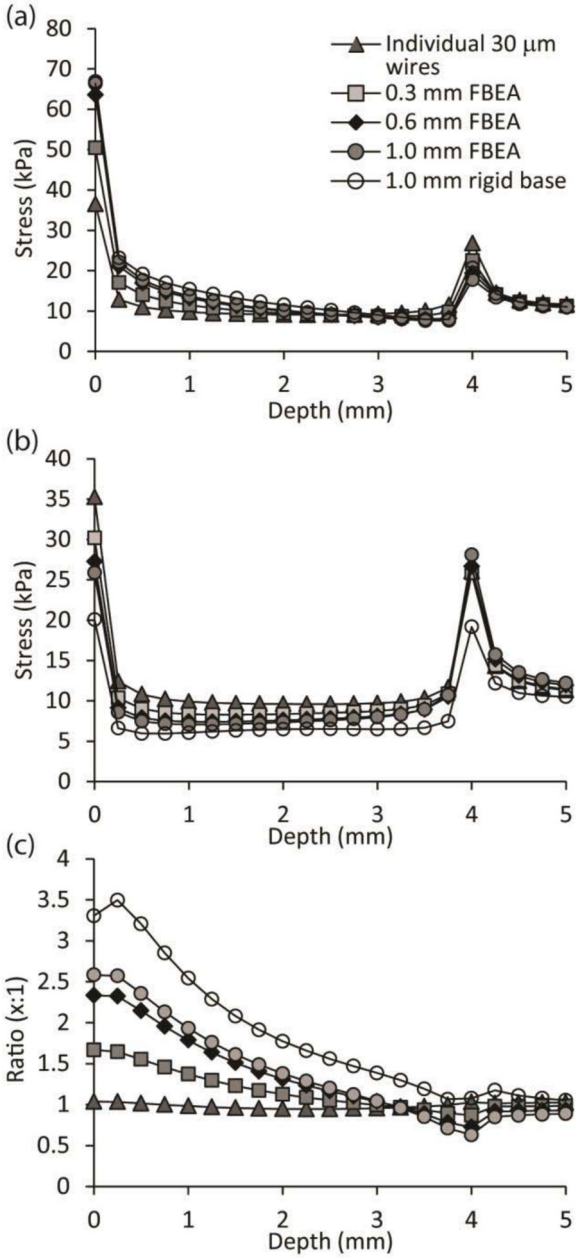


**Fig. 6. Stress analysis**

Modeled stress along the electrode/cord interface during 12% elongation, 10 μm from the electrode. The abscissa of the x axis corresponds to the surface of the cord, while the tip of the electrode is at 4.0 mm. The stress on the outer pair of electrodes (averaged) is shown in (a), and the stress on the inner pair of electrodes (averaged) is shown in (b). The ratio of stress between the outer and inner electrodes is shown in (c).